Trans. Japan Soc. Aero. Space Sci.
Vol. 53, No. 181, pp. 171–179, 2010

Comparison between Hot and Cold Flow Conditions of Turbine Cascade

By Mahmoud M. EL-GENDI,[1)] Katsunori DOI,[1)] Mohammed K. IBRAHIM,[1),2)]
Koichi MORI[1)] and Yoshiaki NAKAMURA[1)]

[1)]*Department of Aerospace Engineering, Nagoya University, Nagoya, Japan*
[2)]*Aerospace Engineering Department, Faculty of Engineering, University of Cairo, Giza, Egypt*

(Received June 16th, 2009)

Flow quantities in the hot and cold flow conditions of a turbine cascade were compared at the same exit isentropic Mach and Reynolds numbers by three-dimensional flow simulations. In the hot flow condition, the total temperature at the inlet was 772 K, and the isothermal temperature of the blade was 540 K. In the cold flow condition, the total temperature at the inlet was 280 K, and the blade was adiabatic. As a result, the cold and hot flow conditions were similar in total and static density in the wake, total and static pressure, velocity, the thicknesses of the viscous and thermal boundary layers, and the amplitude and frequency of the vortex shedding. On the other hand, they were different in static density in the boundary layer, and total and static temperatures. Moreover, the Eckert-Weise effect was observed in the cold flow condition, while energy separation in the wake was observed in the hot flow condition.

Key Words: Turbine Blade, CFD, Adiabatic Condition, Isothermal Condition, Compressible Flow

Nomenclature

δ_t: thickness of thermal boundary layer
δ_v: thickness of viscous boundary layer
γ: specific heat ratio for air
μ: absolute viscosity
ρ: density
ARC: arc length along blade from stagnation point to beginning of trailing edge on pressure or suction side
C: chord length
c: speed of sound
D: thickness of trailing edge=7.43 mm
h: heat transfer coefficient
M: Mach number
n: coordinate along normal direction to surface of blade or flat plate
P: pressure
PS: pressure side of blade
R: specific gas constant for air
r: coordinate along surface of blade, which is originated from the stagnation point as shown in Fig. 2
Re: Reynolds number
S: coordinate along the surface of the blade, originated from center of trailing edge as shown in Fig. 2
SS: suction side of blade
T: temperature
U: resultant velocity
X: tangential axis to camber line at trailing edge
x: axial coordinate (Fig. 1)
Y: transverse axis normal to *X*-axis
y: pitch coordinate (Fig. 1)

Subscripts

δ_t: at edge of thermal boundary layer
δ_v: at edge of viscous boundary layer
∞: reference value for normalization (Appendix A)
1: inlet
2: exit
is: isentropic (Appendix A)
o: total
w: wall

1. Introduction

In general, the efficiency of the gas turbine can be raised by heating the inflow gas to a high temperature. However, a heating system for the inflow gas and a cooling system for the turbine blade must be installed to achieve it.[1)]

To research and develop a gas turbine, it is necessary to simulate the flow through the actual gas turbine by experiments or computations. Additionally, we must decide the heat condition of the simulation relative to the degree of approximation considering objective and cost.

The conditions can be roughly classified into two: The first is the hot flow condition. This condition is very close to that in the real gas turbine because the inlet flow temperature is much higher than the isothermal temperature of the blade. The second is the cold flow condition. This condition approximates that in a real gas turbine because there isn't a significant temperature difference between the inlet flow and blade. The turbine blade can be treated as isothermal in the first approach, but as adiabatic in the second approach. The inlet flow temperature of the first approach is higher than that of the second approach. The heat transfer was taken into account in the first approach but not in the second. There are some experimental challenges to first approach, i.e., the fluid should be heated and the blade should be cooled. If researchers are not interested in the heat transfer process, they use the second approach, which is easier to implement experimentally because they neither heat the flow

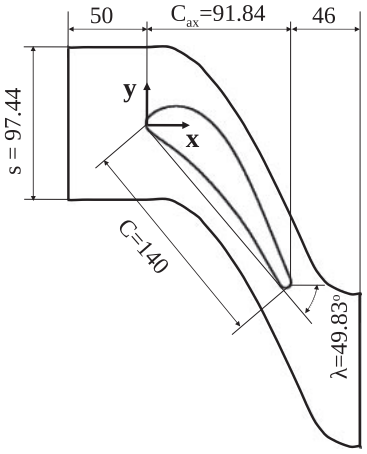

Fig. 1. Investigated cascade (Units: mm).

nor cool the blade. The numerical studies are relevant to the experimental work, i.e., the same boundary conditions. Therefore, when experimental studies adopt one approach, the numerical studies adopt the same approach.

The first hot flow condition approach, is very close to the real case and gives same indication about the heat transfer effect on the blade surface and how flow affects this process. For example, the effect of tip clearance gap on the loss and heat transfer has been investigated intensively experimentally and numerically in the literature.[2–5] C3X and Mark II are famous two-dimensional guide vanes investigated by many researchers.[6–8] Many researchers have investigated the parameters that can affect the prediction of the heat transfer, for example the grid orthogonality,[9] turbulent model,[6,10] and grid density.[11] Generally, these researches focused mainly on the heat transfer not on the flow or aerodynamics.

The second cold flow condition approach, is an approximation of the real case, but investigates the flow phenomena and tendency of flow quantities. For example, Cicatelli and Sieverding[12] considered a turbine cascade with isentropic Mach number, $M_{2,is}$, of 0.4. Sondak and Dorney[13] and Cicalelli et al.[14] numerically investigated this problem by using the same cascade and flow conditions as Cicatelli and Sieverding.[12] Sieverding et al.[15,16] experimentally and El-Gendi et al.[17] numerically investigated the vortex shedding evolution process at $M_{2,is} = 0.79$ on a cascade with half the scale of that used in other research.[12–14,18] El-Gendi et al.[19,20] considered the effect of trailing edge geometry on the base pressure and loss.

A question arises from the above. Can the cold flow condition give us a correct indication of the real case? In other words, does simulating the flow using the second approach agree with that of the first approach? If we maintain the same isentropic Reynolds and Mach numbers, the pressure distributions should be close between the two cases because $M_{2,is}$ is the same, but temperature may have a discrepancy because the heat transfer across the blade exists only in the hot flow condition. To answer this question and check our prediction, we performed numerical simulations to investigate the whole cascade and paid more attention to two different shear layers: the boundary layer, and free shear layer.

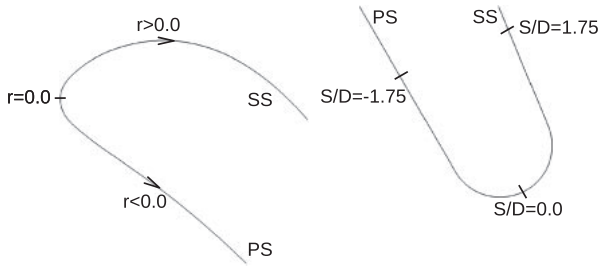

(a) r coordinate (b) S coordinate

Fig. 2. Definition of coordinates along blade surface.

Table 1. Flow conditions.

	P_{o1} (kPa)	T_{o1} (K)	T_w (K)	$M_{2,is}$	$Re_{2,is}$
CC	140.0	280	—	0.79	2.8×10^6
HC	470.0	772	540	0.79	2.8×10^6
PCFD	264.3	772	540	0.90	1.6×10^6

2. Studied Cases

We investigated two cases: the hot case (HC), and the cold case (CC). HC represents results computed by the hot flow condition. CC represents results computed by the cold flow condition. The turbine cascade in both cases is the same as that used in Sieverding et al.[15,16] The blade profile and the cascade dimensions are shown in Fig. 1. The cascade has a chord length (C) of 140 mm, an axial chord (C_{ax}) of 91.84 mm, a pitch (s) of 97.44 mm, and a stagger angle (λ) of 49.83°.

3. Numerical Method

3.1. Computational grid

The O-type grid was used in both cases to reduce skewness of the grid near leading and trailing round edges. The grid has $413 \times 194 \times 50$ grid points; total number of grid points is about 4.0×10^6. The minimum thickness of the grid cell on the blade is 0.002 mm, which is equivalent to $y^+ \approx 1$. The grid spacing along the span direction is constant. The span length of the computational domain is 14.7 mm, which is approximately twice the thickness of the trailing edge and one-tenth of the chord length.

3.2. Boundary conditions

The boundary conditions are shown in Table 1. CC boundary conditions are exactly the same as Sieverding et al.[15] On the other hand, HC has the same exit isentropic Mach number ($M_{2,is}$) and exit isentropic Reynolds number ($Re_{2,is}$), based on chord length, as those CC. In this study, inlet and exit boundary conditions were imposed by the method of characteristics. The non-slip condition was implemented on blade surface. The periodic condition was used in both the pitch and span directions. As a thermal boundary condition on the wall, the isothermal condition was used in HC, but the adiabatic condition was used in CC.

In HC, both temperatures, T_{o1} and T_w, are different from those in an actual jet engine, but their ratio ($T_w/T_{o1} \approx 0.7$) is

close to that in an actual jet engine.[6] In addition, the total temperature at the inlet ($T_{o1} = 772$ K) is lower than 1000 K, so the assumption of a calorically perfect gas is still valid.[21]

3.3. Numerical scheme

Navier-Stokes equations were solved by our in-house code. The cell vertex finite difference method was used for spatial discretization. And, the lower upper symmetric Gauss Seidel (LUSGS) method was used along with the second order dual time method to obtain time accurate results for unsteady flow. In addition, the Roe's flux-difference splitting with E-fix was used to calculate inviscid numerical fluxes, where the second order of accuracy was achieved by the MUSCL scheme with the Van Albada flux limiter. On the other hand, the viscous fluxes were calculated by the central difference method.

The time increment for each iteration was $\Delta t = 3.33 \times 10^{-7}$ s. The time-averaged values in the computational results were calculated using 10,000 iterations, and the vortex shedding frequency was calculated using 16,500 iterations. Every iteration step has five inner iterations for the implicit scheme (time marching).

The calculations were carried out by an eight-processor Linux cluster, and the Message Passing Interface (MPI) was used for parallelization.

3.4. Turbulent model

As a turbulent model, the Delayed Detached Eddy Simulation (DDES[22]) method was used in this study. It is a hybrid scheme that works as a Reynolds Average Navier-Stokes (RANS) model in the region near the wall and as a Large Eddy Simulation (LES) model in the region away from the wall. Unlike RANS models, the DDES model can provide more accurate results for unsteady flows. Unlike LES, DDES does not require a very fine grid near the wall. Furthermore, unlike Detached Eddy Simulation (DES), DDES depends on both the grid spacing and flow quantities to estimate the thickness of the boundary layer where RANS is applied.

4. Validation

Before the main calculations, we calculated two test problems for HC to validate our code.

For the first problem, we simulated the turbulent boundary layer on a heated flat plate. The calculated results were compared to the experimental data measured by Bell.[23] The velocity and temperature in the uniform flow were 17.95 m/s and 20.3°C, respectively. And, the wall temperature was 46.3°C. Figure 3 shows the velocity and static temperature distributions at the point 1.53 m from the leading edge. Both velocity and static temperature distributions have good agreement with the experimental data.[23]

For the second test problem, we simulated the flow around a Mark II blade with a trailing edge modified to a circular shape. This blade was investigated numerically[6,24] and experimentally.[7,8] The boundary conditions are the same as Luo and Lakshminarayana[6] and are shown in Table 1

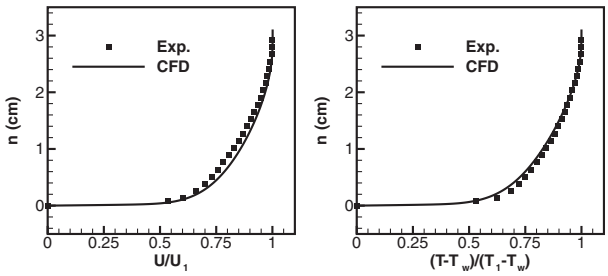

(a) Velocity (b) Static temperature

Fig. 3. Flat plate test (Bell[23]).

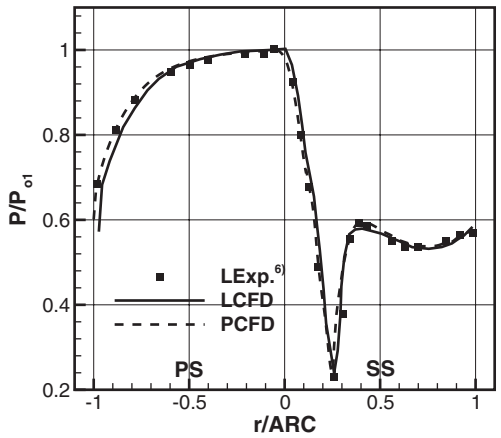

(a) Static pressure

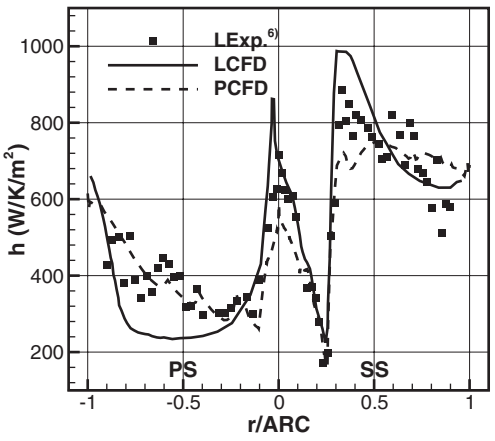

(b) Heat transfer coefficient

Fig. 4. Distributions of pressure and heat transfer coefficient along surface of Mark II blade.

(PCFD). The O-type grid was used, and the total number of grid points is same as used in the main calculations, HC and CC. Figure 4 shows the distributions of the pressure and heat transfer coefficient, where LExp., LCFD, and PCFD represent Luo and Lakshminarayana's experimental results,[6] their computational results,[6] and our computational results, respectively. Pressure is normalized by the total pressure at the inlet (P_{o1}). The abscissa r represents the coordinate along the blade surface. The absolute value of r means the distance from the stagnation point on the leading edge, and the sign of r means the side of the blade. A positive value means SS, and a negative value means PS (Fig. 2).

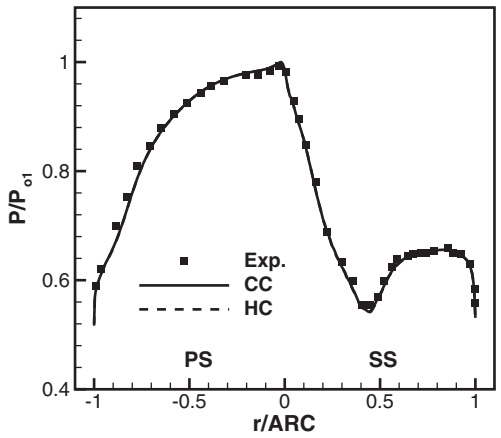

Fig. 5. Distributions of pressure ratio along the blade.

In this PS test problem, we noticed that DDES delays transition excessively. Therefore, the flow was tripped at $r/ARC \approx -0.09$ on the PS in the PCFD.

As shown in Fig. 4, the pressure distribution of our computational result agrees reasonably well with that of the experimental result, Lexp. On the other hand, there is a small discrepancy for the heat transfer coefficient between PCFD and Lexp. For most of SS and PS, the PCFD result falls within the scatter of Lexp.[6] Similarly, Luo and Lakshminarayana's computational result, LCFD, has a discrepancy in the heat transfer coefficient.

Luo and Lakshminarayana[6] also compared three distributions of heat transfer coefficients computed by three k-ϵ models. They showed that there is a discrepancy in results between three turbulent models and all differ from experimental data. In this study, we used a different DDES turbulent model. And our computational result, PCFD, differs from LCFD. Therefore, the heat transfer coefficient distribution may be sensitive to the turbulent model, unlike the pressure distribution.

On the whole, the computational results from the two test problems using our code agreed reasonably with experimental data, which could validate our code. Consequently, this code was used to compute the main problem taking into consideration the discrepancy in the computational results mentioned above.

5. Results and Discussion

5.1. Pressure distribution along blade

Figure 5 shows the distributions of the time-averaged static pressure along the blade in both cases as well as the experimental data[15] for CC, where pressures are normalized by total pressure at inlet, P_{o1}. For CC, the numerical result shows good agreement with the experimental data.[15] The pressure distribution for HC coincides with that for CC, so pressure along the surface of the blade is unaffected by the CC approximation because $M_{2,is}$ is the same.

The pressure gradient along the PS surface is monotonically favorable. However, the SS pressure gradient is favorable in the section of $r/ARC < 0.46$, adverse at $0.46 < r/ARC < 0.7$, negligible at $0.7 < r/ARC < 0.9$, and favorable again at $r/ARC > 0.9$.

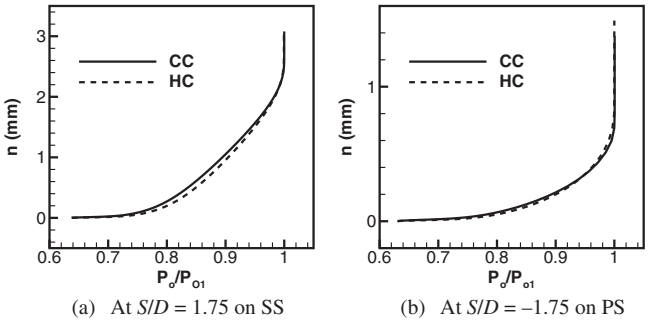

(a) At $S/D = 1.75$ on SS (b) At $S/D = -1.75$ on PS

Fig. 6. Distributions of total pressure in boundary layers.

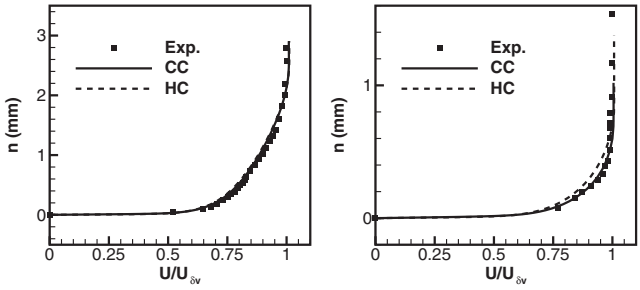

(a) At $S/D = 1.75$ on SS (b) At $S/D = -1.75$ on PS

Fig. 7. Distributions of velocity in boundary layers.

5.2. Boundary layers

Next, we compared flow quantities in boundary layers on PS and SS, i.e., the distribution along the perpendicular direction to the surface on the PS at the point $S/D = -1.75$ ($r/ARC = -0.94$), and on the SS at the point $S/D = 1.75$ ($r/ARC = 0.95$) (Figs. 5 and 2).

For CC and HC, the time-averaged static pressure variation was lower than 0.3% in both boundary layers at $S/D = \pm 1.75$, so static pressure can be considered constant across boundary layers.

Figure 6 shows the distribution of the time-averaged total pressure for CC and HC. There is a little discrepancy between the distribution of the total pressure for HC and that for CC.

Figure 7 shows the time-averaged velocity distributions of our computational results for both cases, and the experimental data[15] for CC. The computational results agree well with the experimental data.[15] Similar to total pressure, there is a small discrepancy between the velocity distribution for CC and HC.

Figure 8 shows the time-averaged static temperature distribution for CC and HC. The distribution of static temperature for CC is very different from HC.

For HC, the static temperature at the wall equals the isothermal value. It is less than outside the boundary layer due to heat transfer across the blade. It increases gradually while parting from the wall until it reaches the static temperature at the edge of the thermal boundary layer.

For CC, the static temperature on the adiabatic wall equals the recovery value. It is higher than outside the bound-

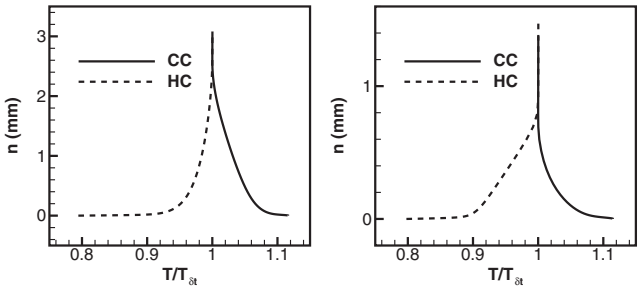

(a) At $S/D = 1.75$ on SS (b) At $S/D = -1.75$ on PS

Fig. 8. Distributions of static temperature in boundary layers.

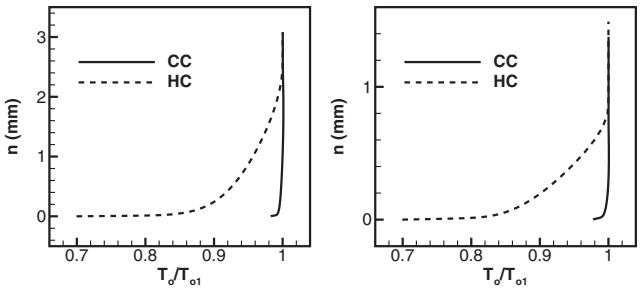

(a) At $S/D = 1.75$ on SS (b) At $S/D = -1.75$ on PS

Fig. 9. Distributions of total temperature in boundary layers.

ary layer due to dissipation resulting from shear stress. It decreases gradually as the dissipation decreases, until it reaches the value at the edge of the thermal boundary layer.

Figure 9 shows the distribution of the time-averaged total temperature for HC and CC. Like static temperature, the distribution of total temperature for CC is very different from HC.

For CC, the total temperature equals the recovery temperature on the adiabatic wall. It increases gradually while parting from the wall and approaches the inlet total temperature due to the work of viscous stress and heat conduction.[25] The average of the normalized total temperature T/T_{o1} across the thermal boundary layer on the adiabatic wall should equal 1.0,[25,26] and the average of our computational result at $S/D = \pm 1.75$ equals approximately 1.0.

On the other hand, for HC, the total temperature at the wall equals the isothermal temperature. It increases gradually while parting from the wall until it reaches the inlet total temperature at the edge of the thermal boundary layer.

Figure 10 shows the distribution of the time-averaged static density for HC and CC. The distribution of the static density for CC is also very different from HC. In both cases on each side, because the static pressure is almost uniform across the boundary layer, the tendencies of the distributions of the static density are opposite to those for static temperature (Fig. 8).

Table 2 shows the thicknesses of the viscous and thermal boundary layers of our computational results in both cases on each side and those for the viscous boundary layers of the experimental data[15] for CC. For CC, there is good agreement between our computational results and the experimental data[15] for viscous boundary layers.

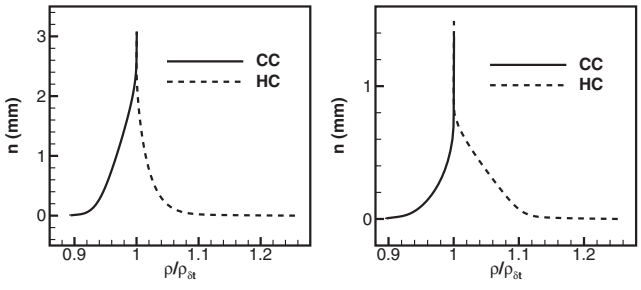

(a) At $S/D = 1.75$ on SS (b) At $S/D = -1.75$ on PS

Fig. 10. Distributions of static density in boundary layers.

Table 2. Thicknesses of boundary layers.

	At $S/D = -1.75$ on PS			At $S/D = 1.75$ on SS			
	Exp	CC	HC	Exp	CC	HC	
δ_v	0.6	0.6	0.7	2.0	2.1	2.1	mm
δ_t		0.8	0.9		2.6	2.6	mm

If the Prandtl number is <1, the thermal boundary layer thickness (δ_t) should be thicker than the viscous boundary layer thickness (δ_v), and vice versa.[26,27] In this study, it equals 0.9 for the turbulent calculations of air. Therefore, the thermal boundary layer thickness (δ_t) is thicker than the viscous boundary layer thickness (δ_v) on each side in each case. The thicknesses of the thermal and viscous boundary layers on each side for CC are close to those for HC. Also, the thicknesses of the viscous and thermal boundary layers on the SS are thicker than those on the PS in both cases.

5.3. Wake

Flow quantities for HC and CC were compared in the free shear layer at $X/D = 2.5$. The angle between the X-axis and the cascade axial direction, x-axis, is 66°. The origin of the X and Y axes was taken at the trailing edge.[28]

The distributions of time-averaged velocity normalized by the speed of sound (c_∞), see Appendix A, for HC and CC are shown in Fig. 11. Like the boundary layer, the velocity distribution for CC is close to that for HC.

The comparison between HC and CC with respect to time-averaged static and total pressure distributions at $X/D = 2.5$ is shown in Fig. 12. Like the boundary layer, the static pressure distribution is identical in both cases, and the total pressure distribution for CC is close to that for HC. The numerical time-averaged static and total temperature distributions for HC and CC are shown in Fig. 13 along with the experimental data[16] for CC. The static and total temperatures for HC are lower than for CC due to the effect of the heat transfer across the blade surface.

Note that the distributions of numerical total pressure and total temperature for CC have a significant quantitative discrepancy from those in the Exp.[16] The turbulent model, DDES, can not model all scales of turbulence correctly, causing this discrepancy.

Using Unsteady RANS (URANS), Leclercq and Doolan[29] observed a similar discrepancy between the experimental and numerical velocity distributions near the wake of an

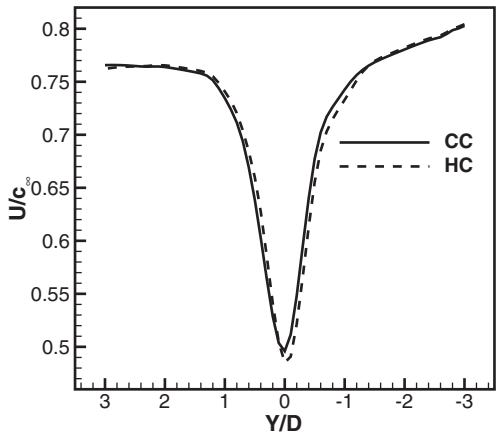

Fig. 11. Time-averaged velocity distributions at $X/D = 2.5$.

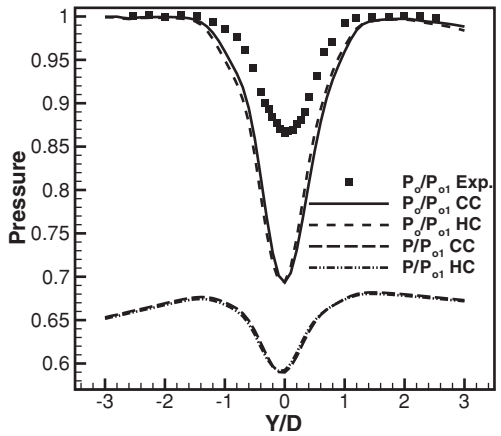

Fig. 12. Time-averaged pressure distributions at $X/D = 2.5$.

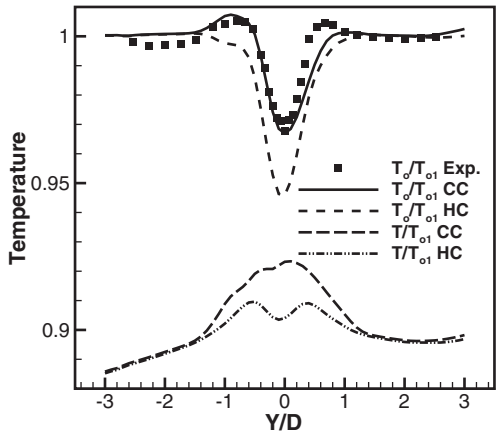

Fig. 13. Time-averaged temperature distributions at $X/D = 2.5$.

isolated blade. They attributed this discrepancy to a three-dimensional effect.[30] In this study, the calculations are three-dimensional, and there is a discrepancy between the experimental and numerical total pressure distributions as shown in Fig. 12.

Using the Baldwin-Lomax turbulent model, Boyle and Ameri[9] observed a discrepancy between the numerical and experimental total pressure values at the 0.42 axial chord behind the blade. They attributed this discrepancy to the conjecture that the amount of diffusion in the wake predicated by the turbulent model is too small. They verified this hypothesis by testing two grids. The coarse grid is more diffusive than the fine one. They noticed that the total pressure values for the coarse grid were greater (closer to experimental results) than those of the fine one. Based on our unpublished results, we investigated the effect of diffusion. We changed the accuracy of the inviscid fluxes from the second order to the first order, which is more diffusive compared to the second order accuracy. Using the first order accuracy, both the total pressure and temperature values increased in the wake. Therefore, although the total pressure results improved, the total temperature results deteriorated, indicating that the turbulent model needs more treatment than increasing the diffusion.

Recently, Mokulys et al.[31] made calculations using three turbulent models: Baldwin-Lomax, Spalart-Allmaras, and k-ω. The turbine cascade and flow conditions are the same as those for CC. Regarding the time-averaged total pressure and temperature distributions at $X/D = 2.5$, the results of each turbulent model differ from the experimental data. In addition, there is a discrepancy between the results of each turbulent model. Also they mentioned that all turbulent models predicted a 30% lower value for total pressure than the experimental value. They attributed this deviation to different mixing process in the calculations than in the experiment. We investigated the effect of turbulent viscosity values by changing the grid. Using DDES, the turbulent viscosity value depends on the cell dimensions, $\max(\Delta x, \Delta y, \Delta z)$. Changing the value of the maximum cell dimension changes the turbulent viscosity value estimated by DDES. We noticed that decreasing the value of the maximum cell dimension by changing the grid resolution increases both the total pressure and temperature. Hence, the total pressure distribution improves and the total temperature distribution deteriorates.

In conclusion, the results of our and other researchers[9,29,31] calculations have good agreement with experimental data qualitatively, but there are quantitative discrepancies. We think that accurate quantitative prediction of flow quantities, T_o and P_o, in this region is a real challenge to turbulent model developers.

As shown in Fig. 13, for CC, both numerical and experimental data show a tendency for total temperature to be lower than T_{o1} at the middle of the wake, exceed T_{o1} at the border of the wake, and approach T_{o1} in the mainstream flow. This is called the Eckert-Weise effect.[16,32] For HC, the total temperature doesn't exceed T_{o1} at the border of the wake so that the Eckert-Weise effect is not observed.

We know that this effect happens mainly due to time-averaged accumulation of instantaneous energy separation phenomenon where the instantaneous total temperature splits into hot and cold spots in the vortex street,[33] and a similar phenomenon is observed in our computational results (Fig. 17). However, we can not predict that the tendency in our computational results must be the Eckert-Weise effect because the heights of the overshoots in the

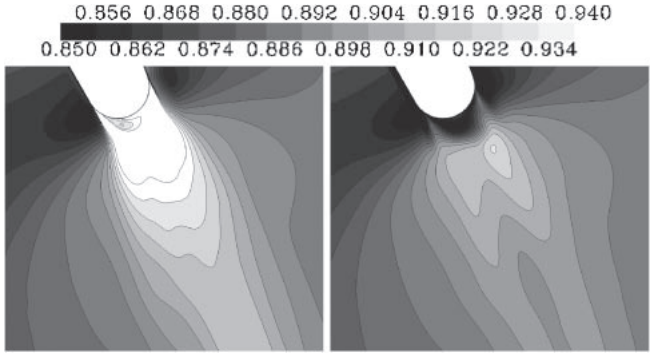

(a) CC (b) HC

Fig. 14. Time-averaged T/T_{o1} contours.

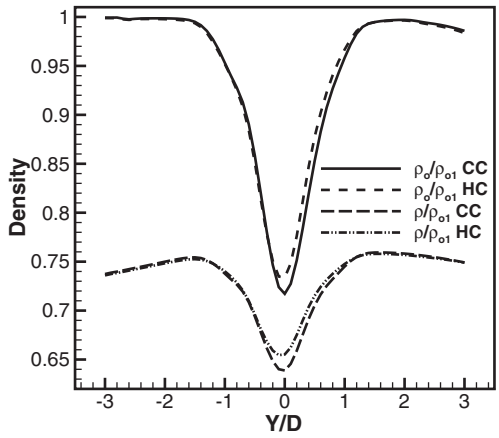

Fig. 15. Time-averaged density distributions at $X/D = 2.5$.

total temperature distribution are comparable with the precision of this numerical simulation.

The time-averaged static temperature for HC has a different tendency from CC. For HC, the static temperature has a moderate value of the wake centerline, and gradually increases and then decreases while moving out. For CC, the static temperature has the highest value of the wake middle, and decreases gradually while moving out.

As shown in Fig. 13, for HC, the static temperature in the wake is higher than in the mainstream despite the wake being downstream of boundary layers cooled by the blade surface. In addition, there are two local maxima in static temperature. To investigate these observations, the static temperature contours in the wake region were calculated. Figure 14 shows the numerical time-averaged static temperature contours for HC and CC.

Near the blade for HC, the static temperature is low due to cooling. The vortex formation is behind the trailing edge. Part of the kinetic energy in the formation region dissipates and converts to heat. The static temperature increases gradually due to dissipation in the formation region in the wake. Therefore, the static temperature in the wake is higher than in the mainstream due to heat generated by the dissipation. For HC, the static temperature near the wake center is decreased by heat transfer on the blade surface, but the wake static temperature is increased by dissipation in the formation region and becomes higher than the mainstream. Therefore, there are two local maxima in the static temperature.

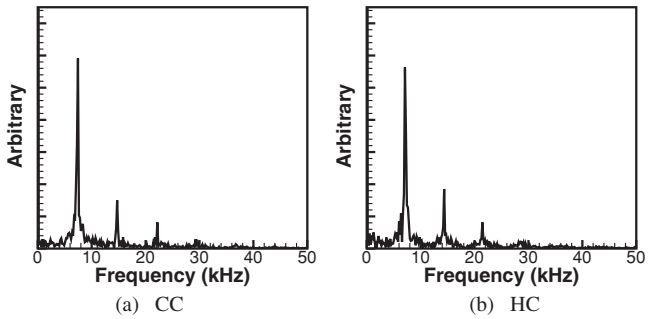

(a) CC (b) HC

Fig. 16. Pressure spectra at $S/D = -0.66$.

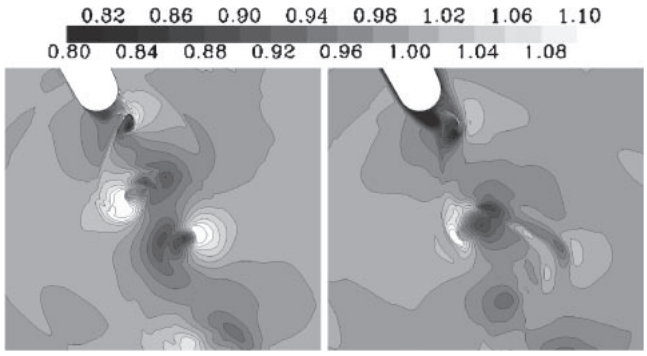

(a) CC (b) HC

Fig. 17. Instantaneous T_o/T_{o1} contours.

For CC, the static temperature near the wake center is increased by dissipation in the boundary layer. Furthermore, the wake static temperature is increased by the dissipation in the formation region. Therefore, the static temperature, T/T_{o1} for CC is higher than for HC (Fig. 13).

Figure 15 shows the numerical time-averaged static and total density distributions for HC and CC. Both the static and total density distributions for CC are close to those for HC.

5.4. Vortex shedding frequency

Figure 16 shows the spectral analysis for the pressure fluctuations at midspan where $S/D = -0.66$ for HC and CC. Both HC and CC have one predominant vortex shedding frequency. for CC, it equals 7.45 kHz, which shows reasonable agreement with the experimentally obtained frequency of 7.37 kHz[15] and 7.6 kHz.[16] On the other hand, it equals 7.09 kHz for HC. In addition, Fig. 16 shows that the pressure amplitude of the predominant frequency for CC is close to that for HC.

5.5. Energy separation in wake

Figure 17 shows the contours of instantaneous total temperature normalized by temperature at the inlet for HC and CC. In both cases, the instantaneous total temperatures in the wake split into hot and cold spots, which is known as the energy separation phenomenon.[32,33] El-Gendi et al.[28] noticed that the combination of the convective and rotational velocities of the vortex makes a main contribution for energy separation. Therefore, the phenomenon is observed in both cases.

6. Conclusion

Numerical simulation of the flow field of a turbine cascade was performed for the hot flow condition where hot gas flows around the isothermal blade, and for the cold flow condition where cold gas flows around the adiabatic blade. The exit isentropic Mach number is 0.79, and the exit isentropic Reynold number is 2.8×10^6 in both cases.

The computational results showed the similarity between the flow field in the cold flow condition and in the hot flow condition for total and static density in the wake, total and static pressure, velocity, thicknesses of the viscous and thermal boundary layers, and the amplitude and frequency of the vortex shedding. On the other hand, they showed the difference between the two conditions for static density in the boundary layer, and total and static temperatures. These results suggest that some indications about flow field in an actual hot flow condition can be obtained by easier experiments in cold flow condition.

In addition, energy separation in the wake was observed in the numerical results for hot flow condition, while the Eckert-Weise effect was observed in the cold flow condition.

Acknowledgments

The first author's Ph.D. program was supported by the Egyptian Ministry of Higher Education. We would like to thank Prof. Sieverding who kindly supplied the blade coordinates. We are also grateful to M. El-Ghandour for his interesting discussions and fruitful advice.

References

1) Han, J., Dutta, S. and Ekkad, S. V.: *Gas Turbine Heat Transfer and Cooling Technology*, Taylor & Francis, New York, 2000.
2) Ameri, A. A.: Heat Transfer and Flow on the Blade Tip of a Gas Turbine Equipped with a Mean-Camberline Strip, *J. Turbomach.*, **123** (2001), pp. 704–708.
3) Ameri, A. A. and Bunker, R. S.: Heat Transfer and Flow on the First-Stage Blade Tip of a Power Generation Gas Turbine: Part 2-Simulation Results, *J. Turbomach.*, **122** (2000), pp. 272–277.
4) Azad, G. S., Han, J., Teng, S. and Boyle, R. J.: Heat Transfer and Pressure Distributions on a Gas Turbine Blade Tip, *J. Turbomach.*, **122** (2000), pp. 717–724.
5) Ameri, A. A., Park, B., Steinthorsson, E. and Rigby, D. L.: Effects of Tip Clearance and Casing Recess on Heat Transfer and Stage Efficiency in Axial Turbines, *J. Turbomach.*, **121** (1999), pp. 683–693.
6) Luo, J. and Lakshminarayana, B.: Numerical Simulation of Turbine Blade Boundary Layer and Heat Transfer and Assessment of Turbulence Models, *ASME J. Turbomach.*, **119** (1997), pp. 794–801.
7) Nealy, D. A., Mihelc, M. S., Hylton, L. D. and Gladden, H. J.: Measurements of Heat Transfer Distribution over the Surfaces of Highly Loaded Turbine Nozzle Guide Vanes, *J. Eng. Gas Turbines Power*, **106** (1984), pp. 149–158.
8) Hylton, L. D., Mihelc, M. S., Turner, E. R., Nealy, D. A. and York, R. E.: Analytical and Experimental Evaluation of the Heat Transfer Distribution over the Surface of Turbine Vanes, NASA CR-168015, 1983.
9) Boyle, R. J. and Ameri, A. A.: Grid Orthogonality Effect on Predicted Turbine Midspan Heat Transfer and Performance, *J. Turbomach.*, **119** (1997), pp. 31–38.
10) Medic, G. and Durbin, P. A.: Toward Improved Prediction of Heat Transfer on Turbine Blades, *J. Turbomach.*, **124** (2002), pp. 187–192.
11) Dorney, D. J. and Davis, R. L.: Navier-Stokes Analysis of Turbine Blade Heat Transfer and Performance, *J. Turbomach.*, **119** (1997), pp. 31–38.
12) Cicatelli, G. and Sieverding, C. H.: The Effect of Vortex Shedding on the Unsteady Pressure Distribution Around the Trailing Edge of a Turbine Blade, *J. Turbomach.*, **119** (1997), pp. 810–819.
13) Sondak, D. and Dorney, D.: Vortex Shedding in a Turbine Cascade, *Int. J. Turbo. Jet Engines*, **16** (1999), pp. 107–126.
14) Manna, M., Mulas, M. and Cicatelli, G.: Vortex Shedding Behind a Blunt Trailing Edge Turbine Blade, *Int. J. Turbo Jet Engine*, **14** (1997), pp. 145–157.
15) Sieverding, C. H., Richard, H. and Desse, J.: Turbine Blade Trailing Edge Flow Characteristics at High Subsonic Outlet Mach Number, *J. Turbomach.*, **125** (2003), pp. 298–309.
16) Sieverding, C. H., Ottolia, D., Bagner, C., Comadoro, A., Brouckaert, J. F. and Desse, J.: Unsteady Turbine Blade Wake Characteristics, *J. Turbomach.*, **126** (2004), pp. 551–559.
17) El-Gendi, M. M., Ibrahim, M. K., Mori, K. and Nakamura, Y.: Numerical Simulation of Trailing Edge Vortex Shedding in a High Subsonic Turbine Cascade, Proceedings of JSASS-KSAS Joint International Symposium on Aerospace Engineering, 2007, pp. 8–11.
18) Sieverding, H., Cicatelli, G., Desse, J. M., Meinke, M. and Zunino, P.: *Experimental and Numerical Investigation of Time Varying Wakes Behind Turbine Blades*, Vieweg, Braunschweig, 1999.
19) El-Gendi, M. M., Ibrahim, M. K., Mori, K. and Nakamura, Y.: Elliptic Trailing Edge for a High Subsonic Turbine Cascade, Proceedings of KSAS-JSASS Joint International Symposium on Aerospace Engineering, 2008, pp. 38–42.
20) El-Gendi, M. M., Ibrahim, M. K., Mori, K. and Nakamura, Y.: Effect of Trailing Edge Geometry on a Turbine Blade Base Pressure, Proceedings of International Symposium on Frontiers of Computational Science, 2008, pp. 197–204.
21) Anderson, J. D.: *Modern Compressible Flow with Historical Perspective*, McGraw Hill, London, 2004.
22) Spalart, P. R., Deck, S., Shur, M. L., Squires, K. D., Strelets, M. K. and Travin, A.: A New Version of Detached-Eddy Simulation, Resistant to Ambiguous Grid Densities, *Theor. Comput. Fluid Dyn.*, **20** (2006), pp. 181–195.
23) Bell, J. B.: Boundary Layer on Heated Plate at Constant Pressure, Proceedings of Computation of Turbulent Boundary Layer, Vol. 2, AFOSR-Stanford, 1968, pp. 282–296.
24) Rahman, F., Visser, J. A. and Morris, R. M.: Capturing Sudden Increase in Heat Transfer on the Suction Side of a Turbine Blade Using a Navier-Stokes Solver, *J. Turbomach.*, **127** (2005), pp. 552–556.
25) Eckert, E. R. G.: Energy Separation in Fluid Streams, *Int. Comm. Heat Mass Transfer*, **13** (1986), pp. 127–143.
26) White, F. M.: *Fluid Mechanics*, McGraw-Hill, New York, 1999.
27) Schlichting, H.: *Boundary-Layer Theory*, McGraw-Hill, New York, 1979.
28) El-Gendi, M. M., Ibrahim, M. K., Mori, K. and Nakamura, Y.: Energy Separation in a High Subsonic Turbine Cascade, *Trans. Jpn. Soc. Aeronaut. Space Sci.*, **52** (2010), pp. 206–212.
29) Leclercq, D. J. and Doolan, C. J.: The Interaction of a Bluff Body with a Vortex Wake, *J. Fluids Struct.*, **25** (2009), pp. 867–888.
30) Roshko, A.: Perspectives on Bluff Body Aerodynamics, *J. Wind Eng. Ind. Aerodyn.*, **49** (1993), pp. 79–100.
31) Mokulys, T., Congiu, F., Rose, M. G. and Abhari, R. S.: Unsteady Numerical Investigation of the Effect of Wakes with Eddy Shedding in Different Axial Turbine Aerofoils, *Proc. IMechE, J. Power Energy*, **223 A** (2009), p. 1001–1016.
32) Carscallen, W. E., Currie, T. C., Hogg, S. I. and Gostelow, J. P.: Measurement and Computation of Energy Separation in the Vortical Wake Flow of a Turbine Nozzle Cascade, *J. Turbomach.*, **121** (1999), pp. 703–708.
33) Kurosaka, M., Gertz, J. B., Graham, J. E., Goodman, J. R., Sundaram, P., Riner, W. C., Kuroda, H. and Hankey, W. L.: Energy Separation in a Vortex Street, *J. Fluid Mech.*, **178** (1987), pp. 1–29.

Appendix A

The isentropic and infinity quantities were calculated from the inlet and exit boundary conditions and isentropic relations.

$$T_\infty = T_{o1}\left(1 + \frac{\gamma - 1}{2} M_{2,is}^2\right)^{-1}$$

$$c_\infty = \sqrt{\gamma R T_\infty}$$

$$M_{2,is} = \sqrt{\frac{2}{\gamma - 1}\left[\left(\frac{P_2}{P_{o1}}\right)^{\frac{1-\gamma}{\gamma}} - 1\right]}$$

$$Re_{2,is} = \frac{(\rho U)_{2,is} C}{\mu}$$

$$(\rho U)_{2,is} = \frac{\gamma M_{2,is} P_{o1}}{\sqrt{\gamma R T_{o1}}}\left(1 + \frac{\gamma - 1}{2} M_{2,is}^2\right)^{\frac{\gamma+1}{2(1-\gamma)}}$$